Assessing the Seasonal Dynamics of Nitrate and Sulfate Aerosols at the South Pole Utilizing Stable Isotopes

Wendell Walters, Greg Michalski, J. Böhlke, Becky Alexander, Joel Savarino, Mark H Thiemens

Assessing the Seasonal Dynamics of Nitrate and Sulfate Aerosols at the South Pole Utilizing Stable Isotopes

Wendell W. Walters[1,2*], Greg Michalski[3,4*], J.K. Böhlke[5], Becky Alexander[6], Joël Savarino[7], and Mark H. Thiemens[8]

[1]Department of Earth, Environmental, and Planetary Sciences, Brown University, Providence, RI, USA

[2]Institute at Brown for Environment and Society, Brown University, Providence, RI, USA.

[3]Department of Earth, Atmospheric, and Planetary Sciences Purdue University, West Lafayette, IN, USA.

[4]Department of Chemistry, Purdue University, West Lafayette, IN, USA.

[5]U.S. Geological Survey, Reston, VA 20192, USA

[6]Univ. Grenoble Alpes, CNRS, IRD, Grenoble INP, IGE, F-38000 Grenoble, France

[7]Department of Atmospheric Sciences, University of Washington, Seattle, WA, USA

[8]Department of Chemistry and Biogeochemistry, University of California, San Diego, La Jolla, CA, USA.

Corresponding author: Wendell W. Walters (wendell_walters@brown.edu) & Greg Michalski (gmichals@purdue.edu)

Key Points:

- The stable isotope compositions of nitrate and sulfate were measured from aerosol samples collected at the South Pole
- Distinct seasonal cycles were found in both concentration and isotopic compositions resulting from changing contributions of emission sources and oxidation chemistry
- The budgets of nitrate and sulfate at the South Pole are complex functions of transport, localized chemistry, biological activity, and meteorological conditions.

Abstract

Atmospheric nitrate (NO_3^- = particulate NO_3^- + gas-phase nitric acid (HNO_3)) and sulfate (SO_4^{2-}) are key molecules that play important roles in numerous atmospheric processes. Here, the seasonal cycles of NO_3^- and total suspended particulate sulfate ($SO_4^{2-}{}_{(TSP)}$) were evaluated at the South Pole from aerosol samples collected weekly for approximately 10-months (January 26 to October 18) in 2002 and analyzed for their concentration and isotopic compositions. Aerosol NO_3^- was largely affected by snowpack emissions in which [NO_3^-] and $\delta^{15}N(NO_3^-)$ were highest (49.3±21.4 ng/m^3, n = 8) and lowest (-47.0±11.7‰, n = 5), respectively, during periods of sunlight in the interior of Antarctica. The seasonal cycle of $\Delta^{17}O(NO_3^-)$ reflected tropospheric chemistry year-round with lower values observed during sunlight periods and higher values observed during dark periods, reflecting shifts from HO_x- to O_3-dominated oxidation chemistry. $SO_4^{2-}{}_{(TSP)}$ concentrations were highest during summer and fall (86.7±73.7 ng/m^3, n =18) and are suggested to be derived from dimethyl sulfide (DMS) emissions supported by $\delta^{34}S(SO_4^{2-})_{(TSP)}$ values (18.5±1.0‰, n=10) near the DMS $\delta^{34}S$ source value. The seasonal cycle of $\Delta^{17}O(SO_4^{2-})_{(TSP)}$ exhibited minima values during summer (0.9±0.1‰; n=5) and maxima during fall (1.3 ± 0.3‰, n =6) and spring (1.6±0.1‰, n=5), indicating a shift from HO_x- to O_3-dominated chemistry in the atmospheric derived SO_4^{2-} component. Overall, the budgets of NO_3^- and $SO_4^{2-}{}_{(TSP)}$ at the South Pole are complex functions of transport, localized chemistry, biological activity, and meteorological conditions, and these results will be important for future interpretations of oxyanions in ice core records in the interior of Antarctica.

1 Introduction

The interior of Antarctica is a unique region to study atmospheric chemistry because of its pristine nature, distinctive climatology, and the potential influence of stratospheric dynamics on

tropospheric chemistry (Hill-Falkenthal et al., 2013; McCabe et al., 2007; Savarino et al., 2007; Shaw, 2010; Wagenbach, 1996). The region is also vital for paleoclimotology studies that relate trace gases (CO_2, CH_4, N_2O) and aerosols, trapped in the polar ice, to past global climate shifts and feedback mechanisms (Alexander et al., 2003; Augustin et al., 2004; Barnola et al., 1987; Legrand et al., 1988; Leuenberger et al., 1992; Meure et al., 2006; Röthlisberger et al., 2000). By measuring changes in greenhouse gas concentrations and their stable isotopic compositions, it is possible to place constraints on the change in sources of these compounds over time (Craig et al., 1988; Friedli et al., 1986; Leuenberger et al., 1992). This is because these gases have small photochemical removal rates, which gives them a long atmospheric lifetime (~10s-100s yr). This allows them to be thoroughly mixed in the global troposphere and incorporated into the ice before removal mechanisms can induce any noticeable isotopic fractionation; thus, the change in isotopic composition can be related, by mass balance, to global source changes.

Utilizing the isotopic composition of nitrate (NO_3^-) and sulfate (SO_4^{2-}) in ice is more complex because both the aerosol and gaseous components of these compounds have atmospheric lifetimes that are considerably shorter (days to months) relative to greenhouse gases. However, these are important oxyanions to study because of the significant role they play in the chemical activity of the atmosphere with important implications for climatic forcing and controls on the atmospheric oxidation budget (Arimoto et al., 2001; Hauglustaine et al., 2014; Haywood & Boucher, 2000; Kiehl et al., 2000). NO_3^- and SO_4^{2-} are formed as secondary products from the oxidation of precursor gases, nitrogen oxides (NO_x = NO + NO_2) and sulfur dioxide (SO_2). Primary sources of SO_4^{2-} also exist including direct emission via sea-salt particles. Due to the conserved mass of S and N between the precursor gases and the oxidized end-products of NO_3^-

and of SO_4^{2-}, the N ($\delta^{15}N$) and S ($\delta^{34}S$) isotopic composition may serve as a proxy providing key information about emissions sources of reduced N and S gases (Hastings et al., 2009; Heaton, 1990; Nielsen, 1974). This may be a helpful tool to constrain N and S emissions sources that remain relatively unclear in the interior of Antarctica (Delmas, 2013; Legrand et al., 2017; Preunkert et al., 2008; Weller et al., 2018). In contrast, the O isotopic composition ($\delta^{18}O$ & $\Delta^{17}O$) is associated with the incorporation of oxygen atoms from various atmospheric oxidants as gaseous precursors (i.e., NO_x and SO_2) are oxidized to NO_3^- or SO_4^{2-} (Alexander et al., 2005; Michalski et al., 2003). The number of isotopic studies of NO_3^- or SO_4^{2-} in polar regions are relatively meager but have received increased attention in recent years, and interpretations of the isotopic signals continue to evolve (Erbland et al., 2013; Frey et al., 2009; Hill-Falkenthal et al., 2013; Ishino et al., 2017; McCabe et al., 2007; Savarino et al., 2007, 2016). However, to utilize stable isotopes in NO_3^- and SO_4^{2-} in a paleoclimate context (i.e., ice core studies) in the interior of Antarctica, we must have a better understanding of the isotopic signatures of these molecules in the polar atmosphere.

Isotopic compositions of NO_3^- can be a useful way to understand sources and oxidation pathways responsible for its formation. Previous works in Antarctica have suggested snowpack photolysis and localized recycling, continental transported anthropogenic derived NO_3^-, and stratospheric inputs as important sources of NO_3^- (Savarino et al., 2007). These NO_3^- inputs have somewhat distinctive $\delta^{15}N$ values of -32.7±8.4‰ (Savarino et al., 2007), 2.5±12.5‰ (Elliott et al., 2009; Freyer, 1978; Heaton, 1987), and estimated 19±3‰ (Savarino et al., 2007), respectively.

Oxidation pathways during NO_3^- formation may be evaluated by using $\Delta^{17}O$ data (McCabe et al., 2007; Michalski et al., 2003; Morin et al., 2007, 2009; Savarino et al., 2007). Briefly, during NO_x oxidation, O atoms of the responsible oxidants are incorporated into the product NO_3^-. Tropospheric O_3 has an elevated $\Delta^{17}O(O_{3bulk})$ near 26‰ (Johnston & Thiemens, 1997; Krankowsky et al., 1995; Vicars et al., 2012; Vicars & Savarino, 2014), with the transferrable O atom of O_3 associated with the terminal end of O_3 (O_{3term}) possessing a $\Delta^{17}O(O_{3term})$ of 39.3±2.0‰ (Vicars & Savarino, 2014). This contrasts with most other atmospheric O-bearing molecules including O_2, H_2O, and RO_2 (or HO_2) that have a $\Delta^{17}O$ near 0‰ (Barkan & Luz, 2005). These differences provide quantitative measures to evaluate NO_x oxidation chemistry involving various contributions from O_3, HO_x, RO_x, and XO (where X = Br or Cl) oxidation pathways (Michalski et al., 2003) and to compare modeled formation pathways (Alexander et al., 2009) with direct observations (Morin et al., 2008; Savarino et al., 2013). The $\Delta^{17}O$ observed in nitrate is a balance between the $\Delta^{17}O$ of NO_2 and the subsequent oxidation pathway resulting in NO_3^-. The $\Delta^{17}O$ of NO_2 should reflect NO_x photochemical cycling between NO-O_3-RO_2 (or HO_2), resulting in expected values near 28 to 39‰ (Morin et al., 2011), representing a NO + O_3 branching ratio of 0.72 to 1.0. Post NO_2 reaction pathways have been assumed to reflect O isotopic mass balance with the associated oxidants, which has been derived in numerous previous works (Alexander et al., 2009; Ishino et al., 2017; Michalski et al., 2003; Morin et al., 2009). Based on this framework, the NO_2 + OH pathway is expected to produce the lowest $\Delta^{17}O(NO_3^-)$ values (17.3 to 25.1‰), while the NO_3 + RH and $XONO_2$ hydrolysis are expected to produce the highest $\Delta^{17}O(NO_3^-)$ values (38.0 to 42.7‰) (Table 1) (Morin et al., 2011). Thus, $\Delta^{17}O(NO_3^-)$ may be useful to further understand oxidation chemistry involving NO_3^- in sensitive polar environments.

Previous studies have suggested biogenic sulfur, sea-salt, continental transported SO_4^{2-} (derived from mineral, continental biogenic, and anthropogenic sources) and stratospheric inputs to be important SO_4^{2-} sources to the interior of Antarctica (Arimoto et al., 2001; Hill-Falkenthal et al., 2013). These sources have reported $\delta^{34}S$ signatures of 18.6±1.9‰ for dimethyl sulfide (DMS) (Patris et al., 2002; Sanusi et al., 2006), 21±0.1‰ for sea-salt SO_4^{2-} (Rees et al., 1978), 3±3‰ for continental derived SO_4^{2-} production (Jenkins & Bao, 2006; Li & Barrie, 1993; Norman et al., 1999), and 2.6±0.3‰ for stratospheric (Castleman Jr et al., 1974), respectively.

$\Delta^{17}O$ analysis of SO_4^{2-} is a well-established tool for assessing SO_2 oxidation formation pathways (Alexander et al., 2005; Jenkins & Bao, 2006; Lee & Thiemens, 2001; Savarino et al., 2000). Briefly, atmospheric SO_2 rapidly attains isotopic equilibrium with H_2O (Holt et al., 1981). Thus, any $\Delta^{17}O$ signature observed in SO_4^{2-} derives from SO_2 oxidation and can be used to assess the relative importance of SO_2 oxidation pathways, allowing for an understanding of the relative importance of aqueous-phase and gas-phase oxidation (Alexander et al., 2005, 2009; Dominguez et al., 2008; Hill-Falkenthal et al., 2013; Lee & Thiemens, 2001; Savarino et al., 2003). Previous works have shown that the $\Delta^{17}O$ signature of $O_{3(bulk)}$ (26‰) (Vicars & Savarino, 2014) and hydrogen peroxide (~1.7‰) (Lyons, 2001; Savarino & Thiemens, 1999) are partially transferred into SO_4^{2-} based on O mass-balance resulting in $\Delta^{17}O(SO_4^{2-})$ values near 6.5‰ and 0.8‰, respectively. However, we note that if O atom transfer occurs from $O_{3(term)}$ as suggested by *ab initio* results (Liu et al., 2001), then the S(IV) + O_3 oxidation pathway could have a $\Delta^{17}O$ as high as 9.3-10.6‰ (Table 1). Gas-phase oxidation via OH will result in a $\Delta^{17}O(SO_4^{2-})$ of 0‰ when isotopic equilibrium with H_2O is reached. Other potentially important aqueous phase SO_2 S(IV) ($=SO_2{\cdot}H_2O + HSO_3^- + SO_3^{2-}$) oxidation pathways include aqueous metal-catalyzed O_2 oxidation, which results in estimated $\Delta^{17}O(SO_4^{2-})$ of -0.1‰ (Barkan & Luz, 2005) and S(IV)

oxidation via hypohalous acids (HOX = HOBr + HOCl) with an expected $\Delta^{17}O(SO_4^{2-})$ of 0‰ due to rapid equilibrium with H_2O (Chen et al., 2016; Fogelman et al., 1989; Troy & Margerum, 1991). Tropospheric S(IV) oxidation via O_3 is the only significant mechanism producing SO_4^{2-} with $\Delta^{17}O$ values >1‰, allowing for quantitative evaluation of the relative contribution of O_3 during SO_4^{2-} formation (Table 1). Thus, $\Delta^{17}O(SO_4^{2-})$ can be a useful tracer for constraining the transport and oxidation chemistry of SO_4^{2-} aerosols at the South Pole. Aqueous-phase formation of SO_4^{2-} is highly pH-dependent, particularly the O_3 pathway; therefore $\Delta^{17}O(SO_4^{2-})$ can provide useful constraints on the oxidation dynamics involving S(IV).

Table 1. Summary of NO_3^- and SO_4^{2-} oxidation pathways and their expected $\Delta^{17}O$ values (adapted from Ishino et al., (2017)). $\Delta^{17}O$ values of NO_3^- are estimated based on box model results of Morin et al., (2011). $\Delta^{17}O$ values of SO_4^{2-} are adapted based on calculations from Savarino et al., (2000).

Species	Oxidation Pathway	$\Delta^{17}O$(oxidant)(‰)	Transferring Factor	$\Delta^{17}O$ Product(‰)
NO_3^-	NO_2 + OH	0 (OH)	2/3(NO_2)	17.3 – 25.1
	N_2O_5 hydrolysis	(37.3 – 42.3) (O_{3term}), 0 (H_2O)	2/3(NO_2) + 1/6(O_{3term})	31.0 – 35.2
	NO_3 + RH	(37.3 – 42.3) (O_{3term})	2/3(NO_2) + 1/3(O_{3term})	38.0 – 42.3
	$XONO_2$ hydrolysis	(37.3 – 42.3) (BrO)	2/3(NO_2) + 1/3(BrO)	38.0 – 42.3
SO_4^{2-}	SO_2 + OH	0 (OH)	-	0
	SO_3^{2-} + $O_{3(aq)}$	37.3 – 42.3 (O_{3term})	1/4(O_{3term})	9.3 – 10.6
	HSO_3^- + $H_2O_{2\,(aq)}$	1.6 (H_2O_2)	1/2(H_2O_2)	0.8
	SO_3^{2-} + O_2(cat. Fe, Mn)	-0.3 (O_2)	1/4(O_2)	-0.1
	SO_3^{2-} + HOX + H_2O	37.3 – 42.3 (HOX)	-	0

Previous isotopic studies have reported the $\Delta^{17}O(NO_3^-)$ at the coast of Antarctica (Dumont d'Urville (DDU), (Ishino et al., 2017; Savarino et al., 2007) and in the interior of

Antarctica (Erbland et al., 2013; Frey et al., 2009; McCabe et al., 2007; Savarino et al., 2016), generally finding a distinctive $\Delta^{17}O$ seasonal cycle that reflects the higher relative contribution of O_3 oxidation and/or stratospheric input during the winter and increased HO_x + RO_x oxidation during the summer. Previous Antarctica $\delta^{15}N(NO_3^-)$ measurements indicate a distinctive seasonal cycle driven by localized snowpack emissions during periods of sunlight (Erbland et al., 2013; Frey et al., 2009; Savarino et al., 2007). Work has also been reported for $\Delta^{17}O(SO_4^{2-})$ at DDU (Ishino et al., 2017) and at Dome C (Hill-Falkenthal et al., 2013), which also find a general seasonal cycle reflecting shifts in gas-phase to aqueous phase oxidation (Hill-Falkenthal et al., 2013). However, the oxidation dynamics involving NO_3^- and SO_4^{2-} over Antarctica, particularly in the interior, are far from solved (Savarino et al., 2016; Hill-Falkenthal et al., 2013). Additionally, $\Delta^{17}O(SO_4^{2-})$ from snow pit samples at the South Pole has recently been shown to have large interannual variation related to El-Nino Southern Oscillations (ENSO) events (Shaheen et al., 2013). To improve understanding of the dynamics associated with NO_3^- and SO_4^{2-} aerosols in the interior of Antarctica, here we present concentration and $\delta^{15}N$, $\delta^{34}S$, $\delta^{18}O$ and $\Delta^{17}O$ measurements of atmospheric NO_3^- (=particulate NO_3^- + $HNO_{3(g)}$) and total suspended particulate SO_4^{2-} ($SO_4^{2-}{}_{(TSP)}$) collected at the South Pole for approximately 10 months in 2002. The dynamics of NO_3^- and $SO_4^{2-}{}_{(TSP)}$ are assessed in terms of source changes ($\delta^{15}N$ and $\delta^{34}S$) and oxidation chemistry ($\Delta^{17}O$ & $\delta^{18}O$). These data will be useful for understanding the seasonal cycling of NO_3^- and $SO_4^{2-}{}_{(TSP)}$ concentrations in the atmosphere at the South Pole, which has a unique feature of the absence of diurnal solar radiation cycle, contrary to Dome C or coastal Antarctic sites.

2 Materials and Methods

2.1 South Pole Meteorology

Antarctica has a unique climate and meteorology that has important implications for atmospheric chemistry as previously well-described (Davis et al., 2004; Helmig et al., 2007; Hill-Falkenthal et al., 2013; Legrand et al., 2009; Stohl & Sodemann, 2010; Wendler & Kodama, 1984). The South Pole is on the continents' interior high-plateau at an elevation of 2,836 meters above sea level that slopes downward towards its perimeter (Wendler & Kodama, 1984). There are six months of continuous sunlight and six months without sunlight. This cycle in sunlight can have a strong influence on chemistry driven by photolysis, in which these reactions shut down completely during the polar winter and can play an important role on localized concentrations of atmospheric oxidants that are often driven by photolysis reactions. Solar radiation is similar during both spring and autumn; however, due to the build-up of photolabile molecules during the winter, solar radiation returning in the spring can create a different chemical environment relative to autumn. In addition, greater amounts of UV radiation reach the troposphere during the spring due to the annual occurrence of stratospheric O_3 depletion during the early spring. The 2002 O_3 hole was characteristically small relative to the previous six years and split into two holes at the end of September due to the appearance of sudden stratospheric warming (Varotsos, 2002). According to the South Pole Station Meteorology Office (http://amrc.ssec.wisc.edu/usap/southpole/), (1) South Pole surface temperatures have a typical annual range between -76 °C and -18 °C with a mean annual temperature of -49.5 °C, (2) there are strong surface inversions especially during the winter, (3) there is generally very little precipitation in Antarctica's interior and the majority consists of ice crystals or diamond dust,

and (4) winds are generally light compared to the coastal regions of Antarctica, and the prevailing direction is from the north.

2.2 Aerosol Collection

Aerosols were collected on pre-cleaned 20.3 × 25.4 cm glass fiber filters fitted onto a high-volume air sampler between January 26 to October 25 in 2002. The glass fiber filter is assumed to collect total atmospheric nitrate (i.e. particulate nitrate ($p\text{-}NO_3^-$) + nitric acid (HNO_3)) as previously suggested (Frey et al., 2009). The sampler was located on the roof of the Atmospheric Research Observatory (ARO), which is a clean sector roughly one km upwind of the South Pole Observatory (SPO) (90.00° S, 59.00° E). Aerosols were collected for seven-day periods with a flow rate of 1 m^3/min at STP, yielding an average pumped air volume of 10,080 m^3 per collected sample. Filters were kept frozen after collection and during shipment for subsequent chemical and isotopic analysis.

2.3 Anion concentrations and Isotopic Characterization

Water soluble aerosol compounds were extracted from the filters using 100 ml of Millipore water and mechanical shaking for 10 minutes. Filter extracts were analyzed for NO_3^-, and SO_4^{2-} concentrations by ion chromatography (Dionex 2020i). Filter blanks never exceeded 2% of sample; thus, blank corrections were neglected. Based on the concentrations (2-20 ppm), filters were combined by date to ensure at least 8 μmol of NO_3^- and SO_4^{2-} available for isotopic analysis. Adjustments for sea-salt sulfate were not made because of high sodium (Na^+) filter blanks. Previous aerosol SO_4^{2-} measurements in the interior of Antarctica (Dome C) have indicated a relative minor contribution from sea-salt SO_4^{2-} of 3.9 to 6.7% during the summer

(January 15 to March 15, 2010) with an increasing relative contribution during winter of 31.7 to 33.6% (May 15 to Aug 15, 2010) (Hill-Falkenthal et al., 2013). We report $SO_4^{2-}{}_{(TSP)}$ (sea-salt + secondary) and the sea-salt SO_4^{2-} contribution is expected to be relatively small, particularly during the summer, but note that sea-salt contribution is likely higher during winter.

The O isotopes of NO_3^- and SO_4^{2-} were characterized using the thermal decomposition method (Michalski et al., 2002; Savarino et al., 2001). Briefly, the filter extracts were pumped on to a high capacity anion trapping column (Dionex AG15) that was attached to the injection valve of a Dionex 2020i ion chromatography, equipped with anion analytical column (AS9-HC) and a H^+ suppressor membrane column. A 260 mM sodium hydroxide eluent solution was diluted 1:30 with Millipore water and flowed through the system at 0.8 ml/min. Peaks were detected by an online conductivity detector. There three distinctive peaks eluted over a 30-minute separation period; an organic/MSA/Cl^- peak (14 min), NO_3^- (23 min) and SO_4^{2-} (30 min). Thanks to the suppressor membrane column, the sample ions leave the system in their acid forms while the hydroxide eluent is neutralized. The separated H_2SO_4 and HNO_3 were further processed through an offline cation exchange membrane in Ag^+ form to generate $AgNO_3$ and Ag_2SO_4 solutions (10 ml) that were then freeze dried. The silver salts were rehydrated with 70 μL of Millipore water and pipetted into silver boats ($AgNO_3$) or pre-combusted quartz boats (Ag_2SO_4), which were then freeze dried. The $AgNO_3$ and Ag_2SO_4 were then thermally decomposed to evolve O_2 gas that was then analyzed by a dual inlet isotope ratio mass spectrometer (Finnigan-Mat 251). Based on standards of the same size that were processed in a similar manner, the precision of the analysis is ±0.2‰ for $\Delta^{17}O$ and ±2.0‰ for $\delta^{18}O$.

250 During the thermal decomposition of the silver salts, liquid nitrogen traps cryogenically
251 removed the byproduct gases, $NO_{2(g)}$ and $SO_{2(g)}$ (Michalski et al., 2002; Savarino et al., 2001).
252 The $NO_{2(g)}$ aliquots were cryogenically transferred to evacuated glass tubes that were flame-
253 sealed and sent to the USGS stable isotope lab in Reston, Virginia for $\delta^{15}N$ analysis. Samples
254 included aliquots of $NO_{2(g)}$ produced from the nitrate isotopic reference material USGS35. At
255 USGS, sealed tubes containing $NO_{2(g)}$ were cracked under vacuum and transferred cryogenically
256 to quartz-glass tubes containing Cu, Cu_2O, and CaO, which were then flame sealed and baked at
257 850°C and cooled slowly to convert $NO_{2(g)}$ to N_2 and remove traces of H_2O and CO_2 (Bohlke et
258 al., 1993). The baked tubes were cracked under vacuum at the inlet to a Finnigan Delta series
259 IRMS and the N_2 was analyzed in dual-inlet mode against aliquots of N_2 prepared similarly from
260 nitrate isotopic reference materials RSIL-N55 (+3.6‰) and USGS32 (+180‰) with
261 reproducibility of ± 0.1 to 0.2‰. Overall uncertainties were larger because of potential
262 fractionation effects during NO_2 production. We note that all SP samples had a near quantitative
263 conversion of NO_3^- to $NO_{2(g)}$ and thus are expected to result in minimal isotopic fractionation.
264 However, NO_2 generated from USGS35 and analyzed a year later had poor conversion yield (16
265 to 29%) and yielded $\delta^{15}N = -14.0 \pm 0.1$‰, compared to the reported reference value of +2.7 ‰.
266 Thus, there could be uncertainty in our absolute reported $\delta^{15}N$ values, but we expect this to be
267 minimal due to the high conversion yields of our samples. Residual $SO_{2(g)}$ from thermal
268 decomposition was oxidized to SO_4^{2-} using a 30% hydrogen peroxide solution and precipitated
269 as $BaSO_4$. The $BaSO_4$ was mixed with V_2O_5 and $\delta^{34}S$ was determined using TCEA interface and
270 CF-IRMS, with standard deviations of approximately ±0.3‰, based on replicate analysis of
271 international standard reference materials.
272

All isotopic compositions are reported relative to an internal reference material using delta (δ) notation in units of per mil (‰) (Eq. 1):

$$\delta(‰) = 1000\left(\frac{R_{samp}}{R_{ref}} - 1\right) \quad \text{(Eq. 1)}$$

where R refers to the ratio of the heavy to the light isotope (i.e. $^{15}N/^{14}N$, $^{34}S/^{32}S$, $^{17}O/^{16}O$, and $^{18}O/^{16}O$) for the sample or reference, respectively. Atmospheric nitrogen (N_2), Vienna Cañon Diablo troilite (VCDT), and Vienna Standard Mean Ocean Water (VSMOW) are the established international delta-scale references for N, S, and O, respectively. Oxygen mass-independence ($\Delta^{17}O$) was quantified using the linear definition with a mass-dependent coefficient of 0.52, which is approximately representative of O mass-dependent coefficients expected and observed in nature (Eq. 2):

$$\Delta^{17}O = \delta^{17}O - 0.52 \times \delta^{18}O \quad \text{(Eq. 2)}$$

We note that the exact O mass-dependent coefficient will depend on specific equilibrium or kinetic processes, which will have different $\ln(1 + \delta^{17}O)$ versus $\ln(1 + \delta^{18}O)$ relationships with slopes between 0.5 and 0.531 (Young et al., 2002). However, a co-efficient of 0.52 was chosen to be consistent with similar previously published works (Alexander et al., 2004; Michalski et al., 2003; Morin et al., 2007; Savarino et al., 2007) and because it represents a reasonable average of O mass-dependent coefficients expected and observed in nature (Barkan & Luz, 2003; Kaiser et al., 2004; Weston Jr, 2006).

2.4 Complementary Analysis

Air-mass back trajectories arriving at the South Pole were analyzed using NOAA's HYSPLIT (Hybrid Single-Particle Lagrangian Integrated Trajectory) model (Stein et al., 2015).

The model was initiated using the reanalysis meteorology in a regular 2.5° × 2.5° longitude-latitude grid. Seven-day backward trajectories were computed for air masses arriving at the South Pole at an altitude of 3,000 m above sea-level every 5 days for the entire sampling period (January 26 to October 25 in 2002). Ancillary data including temperature, relative humidity, solar irradiance, and [O_3] data for 2002 were obtained from the South Pole Observatory (NOAA) (https://www.esrl.noaa.gov/gmd/dv/data/index.php?site=SPO) and used for statistical analysis.

3 Results

3.1 Concentrations

Weekly measured [NO_3^-] and [SO_4^{2-}]$_{(TSP)}$ are displayed in Figs. 1 and 2, respectively. Overall, both [NO_3^-] and [SO_4^{2-}]$_{(TSP)}$ were quite variable ranging from 3.6 to 87.2 ng/m^3 and 6.5 to 266.3 ng/m^3, respectively. Linear regression correlations between measured concentrations and reported ancillary data (averaged over one-week aerosol collection periods) are reported separately for [NO_3^-] and [SO_4^{2-}]$_{(TSP)}$ as correlation matrices in the Supporting Information (Table S1 and S2). Overall, strong correlations are found between [NO_3^-] and solar irradiance (R^2 = 0.72), while temperature is found to strongly correlate with [SO_4^{2-}]$_{(TSP)}$ (R^2 = 0.67) (Table S1 and S2). Temporal analyses of [NO_3^-] and [SO_4^{2-}]$_{(TSP)}$ indicate somewhat similar seasonal cycles, in which concentrations are generally highest during the summer and lowest during winter (Fig. 1 and 2). However, because [NO_3^-] and [SO_4^{2-}]$_{(TSP)}$ were not strongly correlated (R^2 = 0.29), we will present their results separately. Seven-day back trajectory analysis indicates that air masses tend to derive over the interior of Antarctica (Fig. 3). Slight seasonal variations are observed in which autumn (April to July) and winter (July to October) seven-day back trajectories indicate that some air masses may have traveled over the northern coastal regions of

Antarctica before arriving at SPO, while air masses in summer (Jan to April) and spring (October to sampling end (October 25, 2002)) circulate entirely over the interior of Antarctica (Fig. 3).

3.1.1 $[NO_3^-]$

At the beginning of the year (January to March), $[NO_3^-]$ reached a maximum concentration of 86.2 ng/m^3 in late January and then decreased rapidly to a background concentration of approximately 5.0 ng/m^3 in early March. This strong decline in $[NO_3^-]$ overlaps with decreasing local solar irradiance. The background $[NO_3^-]$ is maintained until early July, in which $[NO_3^-]$ concentrations slowly increase until the end of the sampling period (October 25, 2002), reaching a value of approximately 16.5 ng/m^3. With the onset of solar irradiation at the start of October, NO_3^- is found to rapidly increase until sampling ended. The observed seasonal pattern in $[NO_3^-]$ is similar to that previously reported for atmospheric NO_3^- collected at the South Pole (McCabe et al., 2007), Dome C (Erbland et al., 2013; Frey et al., 2009), and along the coast of Antarctica at Dumont d'Urville (DDU) (Ishino et al., 2017; Savarino et al., 2007).

3.1.2 $[SO_4^{2-}]_{(TSP)}$

At the beginning of the year, $[SO_4^{2-}]_{(TSP)}$ was relatively elevated and reached a maximum of 211.4 ng/m^3 during mid-February and then slowly decreased to a baseline value of approximately 15 ng/m^3 in late April. This baseline $[SO_4^{2-}]_{(TSP)}$ concentration was maintained until mid-September. Subsequently, $[SO_4^{2-}]_{(TSP)}$ increased slightly and reached a value of 67.5 ng/m^3 in the final sample (October 25, 2002). The observed $[SO_4^{2-}]$ seasonal cycle is consistent with previously reported measurements at Dome C (Hill-Falkenthal et al., 2013) and at DDU (Ishino et al., 2017).

342

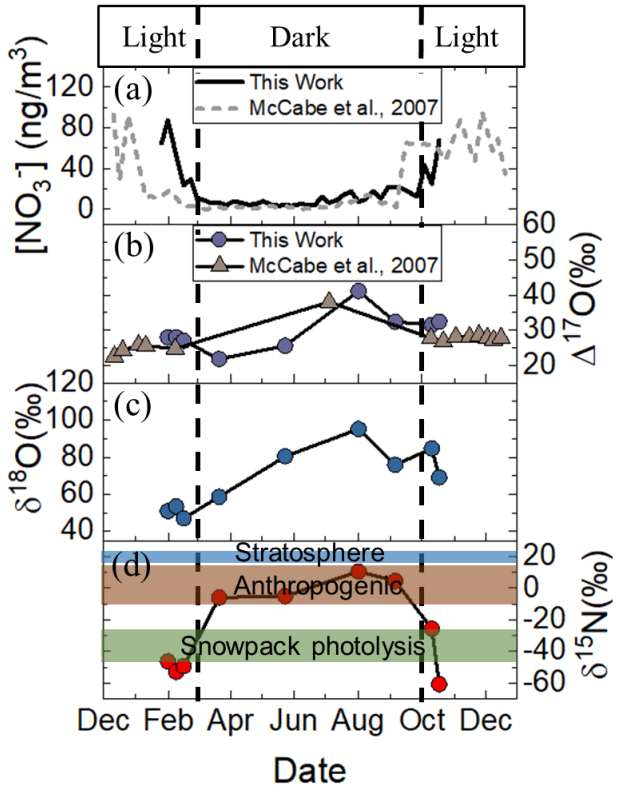

343 **Fig. 1.** Seasonal variation of atmospheric NO_3^- collected at the South Pole in 2002 including (a)
344 concentrations, (b) $\Delta^{17}O(NO_3^-)$, (c) $\delta^{18}O(NO_3^-)$, and (d) $\delta^{15}N(NO_3^-)$. A comparison between
345 previously reported NO_3^- concentration and $\Delta^{17}O$ from aerosols collected at the South Pole
346 (12/1/03 to 12/01/04) is shown in (a) and (b) (McCabe et al., 2007). Ranges of potential $\delta^{15}N$
347 (NO_3^-) sources are indicated in (d) including stratospheric inputs (19±3‰; (Savarino et al.,
348 2007), continental transported anthropogenic derived NO_3^- (2.5±12.5‰; Elliott et al., 2009;
349 Freyer, 1978; Heaton, 1987), and localized recycling of NO_3^- during periods of snowpack
350 photolysis (-32.7±8.4‰; (Berhanu et al., 2015; Berhanu et al., 2014; Savarino et al., 2007)).
351 Periods of constant sunlight and darkness at the South Pole are separated by the black dashed
352 lines.

353

354

355

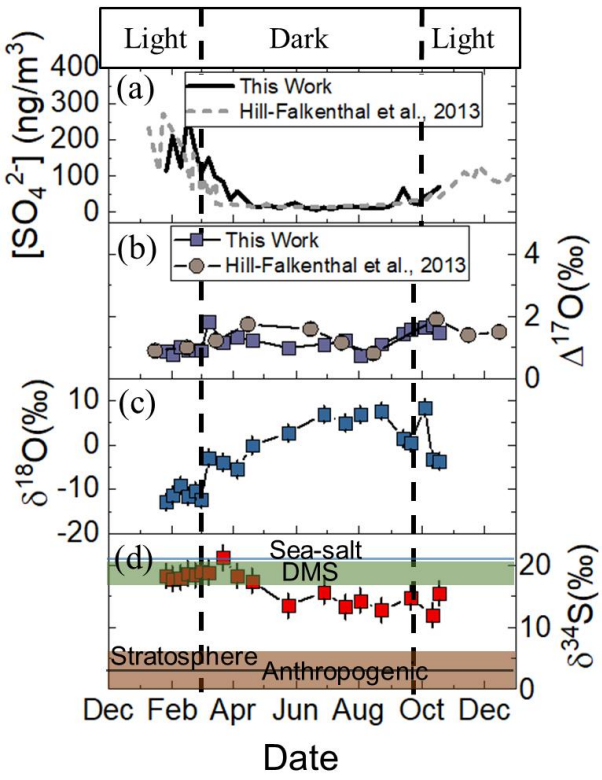

356 **Fig. 2.** Seasonal variations of atmospheric $SO_4^{2-}{}_{(TSP)}$ collected from aerosols in 2002 at the
357 South Pole including (a) concentrations, (b) $\Delta^{17}O(SO_4^{2-}{}_{(TSP)})$, (c) $\delta^{18}O(SO_4^{2-}{}_{(TSP)})$, and (d)
358 $\delta^{34}S(SO_4^{2-}{}_{(TSP)})$. A comparison between previously reported $SO_4^{2-}{}_{(TSP)}$ concentrations and
359 $\Delta^{17}O(SO_4^{2-}{}_{(TSP)})$ from aerosols collected at Dome C (2010) is shown in (a) and (b) (Hill-
360 Falkenthal et al., 2013). Ranges of typical $\delta^{34}S(SO_4^{2-})$ sources are indicated in (d) including sea-
361 salt SO_4^{2-} (21±0.1‰; Rees et al., 1978), DMS (18.6±1.9‰; Patris et al., 2002; Sanusi et al.,
362 2006)), long-range transport of continental SO_4^{2-} derived from anthropogenic emissions (3±3‰
363 (Jenkins & Bao, 2006; Li & Barrie, 1993; Norman et al., 1999), and stratospheric SO_4^{2-} input
364 (2.6±0.3‰; (Castleman Jr et al., 1974)). Periods of constant sunlight and darkness at the South
365 Pole are separated by the black dashed lines.

366

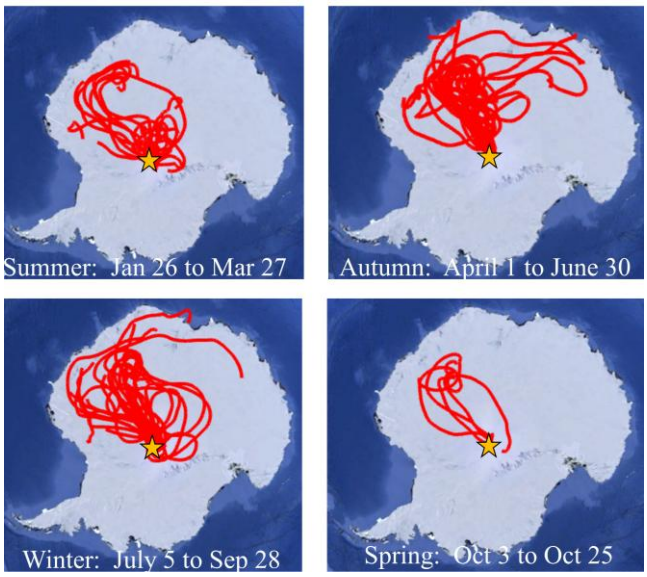

367

368

369 **Fig. 3.** HYSPLIT seven-day back trajectory analysis at the South Pole Observatory (90.00° S,
370 59.00° E; indicated by star) for our sampling period of January 26 to October 25 in 2002 and
371 sorted by season.

372

373 **3.2 Isotopic Compositions**

374 **3.2.1 Nitrate**

375 Nine measurements of the isotopic composition of nitrate were made from the collected
376 samples, which are summarized in Table 2 with average South Polar Observatory data
377 (https://www.esrl.noaa.gov/gmd/dv/data/index.php?site=SPO). The $\delta^{15}N(NO_3^-)$ ranged from -
378 60.8 to 10.5‰ (Fig. 1). The observed $\delta^{15}N(NO_3^-)$ range is consistent with previous $\delta^{15}N$
379 measurements of NO_3^- collected in coastal Antarctica that ranged from -46.9 to 10.8‰ (Savarino
380 et al., 2007) and at Dome C ranging from -35 to 13‰ (Frey et al., 2009), which generally falls

within the ranges of the expected NO_3^- sources that includes snowpack photolysis and localized recycling (-32.7±8.4‰) (Berhanu et al., 2015; Berhanu et al., 2014; Savarino et al., 2007), long range transport of continental NO_3^- (2.5±12.5‰) (Elliott et al., 2009; Freyer, 1978; Heaton, 1987), and stratospheric inputs (estimated 19±3‰) (Savarino et al., 2007) (Fig. 1). Multi-factorial analysis indicates strong linear correlations between $\delta^{15}N$ and $[NO_3^-]$ ($R^2 = 0.66$) and solar irradiance ($R^2 = 0.80$) (Table S1). These correlations likely explain the $\delta^{15}N(NO_3^-)$ seasonal cycle observed in Fig. 1, in which lowest $\delta^{15}N(NO_3^-)$ values are observed during periods of sunlight indicating the importance of snowpack emissions and localized photochemical recycling, while highest $\delta^{15}N(NO_3^-)$ are found during periods of darkness (Fig. 1), which is similar to the seasonal variability previously reported at the coast (Savarino et al., 2007) and in the interior of Antarctica (Erbland et al., 2013; Frey et al., 2009).

Large variability was observed in $\delta^{18}O(NO_3^-)$ and $\Delta^{17}O(NO_3^-)$ that ranged from 47.0 to 95.1‰ and 21.8 to 41.1‰, respectively (Fig. 1). These ranges of values are consistent with previously reported NO_3^- measurements in Antarctica that ranged from 60 to 111‰ and 20.0 to 43.1‰ for $\delta^{18}O$ and $\Delta^{17}O$, respectively (Savarino et al., 2007). Multifactorial analysis indicates strong relationships between $\delta^{18}O$ and temperature ($R^2 = 0.82$), relative humidity ($R^2 = 0.90$), and O_3 mixing ratio ($R^2 = 0.72$) (Table S1). These relationships may be linked by the strong $\delta^{18}O(NO_3^-)$ seasonal pattern, in which values were lowest during the summer and late spring and highest during winter and early spring. Multifactorial analysis found $\Delta^{17}O(NO_3^-)$ to only strongly correlate with O_3 mixing ratio ($R^2 = 0.67$) (Table S1). A comparison between $\delta^{18}O$ and $\Delta^{17}O$ indicates a slight linear correlation ($R^2 = 0.46$) (Table S1). This modest correlation might indicate that the O isotopic composition of the collected nitrate was not a simple mixture

404 between two atmospheric oxidants as previously observed at DDU (Savarino et al., 2007) and
405 Summit, Greenland (Fibiger et al., 2016) but instead may have been influenced by multiple
406 atmospheric oxidants with distinct $\delta^{18}O$ and $\Delta^{17}O$ spaces that were incorporated into atmospheric
407 NO_3^- through NO_x oxidation (Michalski et al., 2012) (Fig. 4).

408

409

410

411 **Table 2.** Summary of average [NO_3^-] (at STP), temperature (Temp), relative humidity (RH), solar radiation, and
412 [O_3], for each collection period corresponding to NO_3^- isotopic composition measurement (see text for details).
413 Parentheses indicate ±1σ for the indicated collection period.
414

Collection Date	Avg [NO_3^-] (ng/m^3)	Temp (°C)*	RH(%)*	Solar Irradiance (W/m^2)*	[O_3] (ppb_v)*	$\delta^{15}N$(±2‰)	$\delta^{18}O$(±2‰)	$\Delta^{17}O$(±0.2‰)
01/26 - 02/09	76.1	-36.4 (2.0)	68.8 (4.0)	265.2 (81.1)	22.6 (3.6)	-46.3	51.0	27.9
02/09 - 02/16	53.0	-38.7 (2.4)	69.4 (5.4)	209.6 (34.9)	20.8 (1.1)	-53.0	53.5	28.0
02/16 - 02/23	24.0	-39.3 (6.2)	70.3 (5)	170.1 (21.3)	20.4 (1)	-49.4	47.0	26.9
02/23 - 03/29	12.3	-49.8 (6.2)	68.4 (5.1)	47.0 (42.9)	20.7 (1.4)	-5.9	58.7	21.8
03/29 - 05/31	5.5	-53.4 (9.3)	65.5 (6.0)	0(0)	25.9 (3.0)	-5.1	80.4	25.6
07/26 - 08/09	12.5	-57.0 (6.7)	64.4 (5.4)	0(0)	34.3 (1.0)	10.5	95.1	41.1
08/09 - 09/13	16.4	-56.8 (9.3)	65.5 (5.8)	0(0)	33.9 (1.6)	4.6	75.9	32.3
10/11 - 10/18	25.3	-55.1 (1.8)	64.2 (2.6)	126.6 (24.5)	30.8 (1.2)	-25.7	84.6	31.4
10/18 - 10/25	67.6	-49.2 (3.6)	68.5 (4.2)	148.3 (25.5)	31.4 (0.8)	-60.8	69.0	32.4

415
416 *data obtained from the South Pole Observatory (NOAA) (https://www.esrl.noaa.gov/gmd/dv/data/index.php?site=SPO)
417

418

419

420

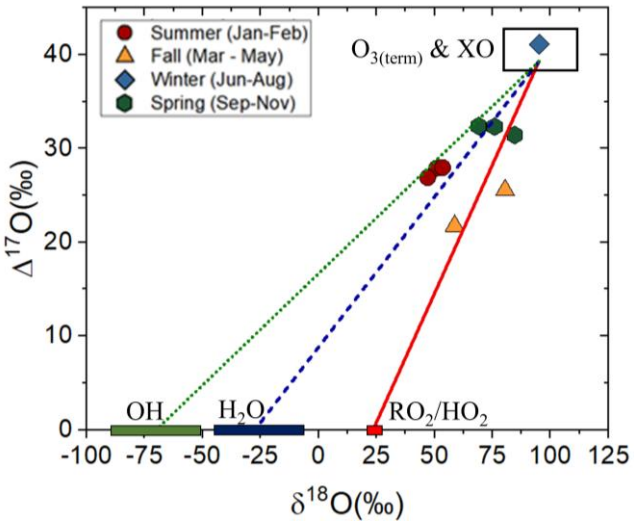

Fig. 4. Relationship between $\delta^{18}O$ and $\Delta^{17}O$ for collected NO_3^- sorted by season displayed with the high $\delta^{18}O$-$\Delta^{17}O$ end member, $O_{3(term.)}$/XO ($\delta^{18}O$ = 95 – 115‰ (Johnston & Thiemens, 1997) and $\Delta^{17}O$ = 39.3‰ (Vicars & Savarino, 2014) and its mixing relations with other important tropospheric O bearing atmospheric molecules including RO_2/HO_2 ($\delta^{18}O$ ~ 23.5‰ and $\Delta^{17}O$ ~ 0‰), H_2O ($\delta^{18}O$ = -40‰ and $\Delta^{17}O$ = 0‰, and OH ($\delta^{18}O$ = -80‰ and $\Delta^{17}O$ = 0‰) (Michalski et al., 2012).

3.2.2 Sulfate

Measured $\delta^{34}S(SO_4^{2-})_{(TSP)}$ was found to range from 11.9 to 21.2‰ (Table 3), which is a similar range to recently reported $\delta^{34}S(SO_4^{2-})_{NSS}$ in the Southern Ocean of 6.0 to 19.0‰ (Li et al., 2018). These ranges of values are near the $\delta^{34}S$ values of the presumed major SO_4^{2-} sources including: dimethyl sulfide emissions = 18.6±1.9‰ (Patris et al., 2002; Sanusi et al., 2006), sea-salt SO_4^{2-} = 21±0.1‰ (Rees et al., 1978), continental SO_4^{2-} (3±3‰) (Jenkins & Bao, 2006; Li & Barrie, 1993; Norman et al., 1999), and stratospheric SO_4^{2-} = 2.6±0.3‰ (Castleman Jr et al.,

437 1974). There is a strong $\delta^{34}S(SO_4^{2-})_{(TSP)}$ seasonal cycle, with highest values (17.7 to 21.2‰)
438 near the beginning of year between January and April. After reaching a peak value of 21.2‰ at
439 the end of March, $\delta^{34}S(SO_4^{2-})_{(TSP)}$ decreased to baseline value between 13 and 15‰ that
440 remained relatively constant with an average of 13.9 ± 1.2‰ (n = 8) until our SO_4^{2-} collection
441 period ended (mid-October).
442
443 Measured $\Delta^{17}O(SO_4^{2-})_{(TSP)}$ values had a narrow range from 0.8 to 1.8‰ (Table 3). Peaks
444 in $\Delta^{17}O(SO_4^{2-})_{(TSP)}$ occurred during sampling between March to May and August to mid-October
445 with average values of 1.4 ± 0.2‰ (n = 4) and 1.6 ± 0.1‰ (n = 3), respectively. Since these
446 values are greater than 1‰, contributions from O_3 aqueous phase oxidation pathway are
447 expected (Alexander et al., 2005) (Fig. 5). The observed $\Delta^{17}O(SO_4^{2-})_{(TSP)}$ profile is similar to
448 that previously observed at Dome C (Hill-Falkenthal et al., 2013) with corrections made to
449 account for sea-salt influence to be consistent with our data (Fig. 2). Measured $\delta^{18}O(SO_4^{2-})_{(TSP)}$
450 ranged from -12.8 to 8.5‰ with a mass-weighted value of -7.3‰ (Table 3). Generally,
451 $\delta^{18}O(SO_4^{2-})_{(TSP)}$ was lowest during the polar summer and highest during polar winter (Fig. 2).
452 The relationship between $\delta^{18}O(SO_4^{2-})_{(TSP)}$ and $\Delta^{17}O(SO_4^{2-})_{(TSP)}$ is found to weakly correlate (R^2 =
453 0.11) (Fig. 5), which might reflect that $\delta^{18}O(SO_4^{2-})_{(TSP)}$ and $\Delta^{17}O(SO_4^{2-})_{(TSP)}$ was influenced by
454 mixing between SO_2 and several different atmospheric oxidations (e.g. O_3, O_2, H_2O_2) as well as a
455 mixture of primary (e.g. sea-salt) and secondary SO_4^{2-} with distinct $\delta^{18}O$-$\Delta^{17}O$ spaces, as
456 previously suggested from South Pole snow pit samples (Shaheen et al., 2013). Strong
457 correlations were observed between $\delta^{18}O(SO_4^{2-})_{(TSP)}$ and temperature (R^2 =0.59) and O_3
458 concentration (R^2 =0.81) recorded at the South Pole Observatory Station. These strong
459 correlations were not observed between $\Delta^{17}O(SO_4^{2-})_{(TSP)}$ and temperature (R^2 =0.15) and O_3

460 concentration (R^2 =0.09) (Table S2), which isn't surprising because aqueous-phase O_3 oxidation

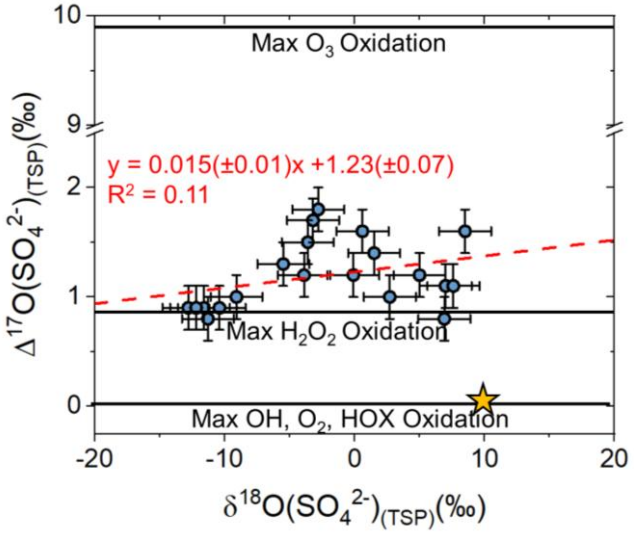

461 is limited by pH.

462

463 **Fig. 5.** Relationship between $\delta^{18}O$ and $\Delta^{17}O$ for collected $SO_4^{2-}{}_{(TSP)}$ (blue points) along with a linear regression of

464 the data (red dashed line; R^2 = 0.11). The isotopic composition of sea-salt sulfate is indicated by the yellow star.

465

466

467

468

469

470

471

472

473

474

475

476 **Table 3.** Summary of average $[SO_4^{2-}]_{(TSP)}$, temperature (Temp), relative humidity (RH), solar radiation, and $[O_3]$ for
477 each collection period corresponding to $SO_4^{2-}{}_{(TSP)}$ isotopic composition measurement (see text for details).
478 Parentheses indicate ±1σ for the indicated collection period.
479

Collection Date	Avg [p-SO_4^{2-}] (ng/m^3)	Temp (°C)*	RH(%)*	Solar Irradiance (W/m^2)*	[O_3] (ppb_v)*	$\delta^{34}S$(±0.3‰)	$\delta^{18}O$(±2‰)	$\Delta^{17}O$(±0.2‰)
1/26 - 2/1	115.3	-35.2 (2.5)	71.9 (4.3)	301.1 (36.6)	22.6 (3.6)	18.3	-12.8	0.9
2/1 - 2/9	211.4	-37.2 (0.9)	66.7 (1.7)	273.7 (19.1)	22 (3.4)	17.7	-11.3	0.8
2/9 - 2/16	124.8	-38.7 (2.4)	69.4 (5.4)	209.6 (34.9)	20.8 (1.1)	18.0	-9.1	1.0
2/16 - 2/23	266.3	-39.3 (6.2)	70.3 (5)	170.1 (21.3)	20.4 (1)	18.6	-11.6	0.9
2/23 - 3/1	172.8	-46.2 (3.7)	68.4 (6.4)	106.7 (30)	20.5 (1.2)	18.3	-10.4	0.9
3/1 - 3/8	107.8	-47.4 (4.5)	69.8 (2.5)	82.9 (18.7)	19.8 (1.4)	18.9	-12.2	0.9
3/8 - 3/22	124.9	-49.3 (5.4)	69.5 (4.3)	24.9 (15.5)	21.4 (1.4)	18.8	-2.8	1.8
3/22 - 4/5	59.9	-52.9 (10)	65.8 (6.7)	1.5 (1.8)	22.6 (0.8)	21.2	-3.9	1.2
4/5 - 4/19	47.5	-50.1 (9)	66.6 (4.7)	0 (0)	24.1 (1)	18.2	-5.5	1.3
4/19 - 5/24	15.5	-57.9 (6)	63.3 (4.7)	0 (0)	27.9 (2.3)	17.4	-0.1	1.2
5/24 - 6/28	17.1	-59.4 (8.7)	64.1 (6)	0 (0)	32.3 (1.1)	13.5	2.7	1.0
6/28 - 7/19	13.0	-53.7 (8.8)	67 (7.7)	0 (0)	34.1 (0.7)	15.6	7.0	1.1
7/19 - 8/2	16.1	-56.5 (8.3)	64.9 (6.4)	0 (0)	34.4 (1.1)	13.3	5.0	1.2
8/2 - 8/23	12.5	-55.7 (10)	65.2 (6.1)	0 (0)	34.4 (1.3)	14.3	6.9	0.8
8/23 - 9/13	18.5	-57.8 (7.4)	65.2 (5)	0 (0)	33.4 (1.5)	12.7	7.6	1.1
9/13 - 9/20	67.1	-54.8 (7.6)	64.9 (3.6)	1.2 (1)	32.4 (1)	--	1.5	1.4
9/20 - 10/4	27.9	-59.4 (5.5)	64.5 (4.9)	19.2 (15.8)	32.4 (1.6)	14.7	0.6	1.6
10/4 - 10/11	44.8	-48.4 (6.4)	68.9 (3.8)	62 (23.1)	33.4 (1.2)	--	8.5	1.6
10/11 - 10/18	54.9	-55.1 (1.8)	64.2 (2.6)	126.6 (24.5)	30.8 (1.2)	11.9	-3.2	1.7
10/18 - 10/25	70.5	-49.2 (3.8)	68.5 (4.2)	148.3 (25.5)	31.4 (0.8)	15.4	-3.6	1.5

480
481 *data obtained from the South Pole Observatory (NOAA)

482

483 # 4 Discussion

484 ## 4.1 NO_3^- Seasonal Cycle

485 ### 4.1.1 $\delta^{15}N(NO_3^-)$

486 The strong correlations between solar irradiance at the South Pole and $[NO_3^-]$ ($R^2 = 0.72$)
487 and $\delta^{15}N(NO_3^-)$ ($R^2 = 0.80$) indicate that localized snowpack photolysis played a key role in
488 controlling NO_3^-, which has important implications for the oxidative environment at the South
489 Pole (Chen et al., 2004). During periods of sunlight, $[NO_3^-]$ are found to be highest (45.0±23.6
490 ng/m^3, n = 9) and $\delta^{15}N(NO_3^-)$ are found to be lowest (-47.0±11.7‰, n = 5) (Fig. 1), which is

consistent with other studies in Antarctica (Erbland et al., 2013; Frey et al., 2009; Ishino et al., 2017; Savarino et al., 2007). The extremely low $\delta^{15}N(NO_3^-)$ found during sunlight periods at the South Pole are typically not found in mid-latitudes, but only appears to occur in Antarctica, due to the chemical and physical processes related to snowpack NO_3^- photolysis that has a large N isotopic enrichment factor (ε) near -48‰ (Berhanu et al., 2015; Berhanu et al., 2014). This favors the release of NO_x depleted in ^{15}N and can explain the extremely low $\delta^{15}N(NO_3^-)$ values found during periods of sunlight. The exportation out of the continent ice sheet of this locally produced nitrate with extremely low $\delta^{15}N(NO_3^-)$ values may explain the low $\delta^{15}N$ observed in the Antarctic dry valley (Michalski et al., 2005).

During periods of darkness, $\delta^{15}N(NO_3^-)$ was found to increase to 1.0 ± 6.8‰ (n= 4), reflecting contributions from another source of NO_3^- with a higher $\delta^{15}N$ end-member. This source is likely derived from an increasing importance of long-range transport of continental NO_3^- (Lee et al., 2014) and/or stratospheric NO_3^- denitrification (Savarino et al., 2007) during periods of darkness, with estimated $\delta^{15}N(NO_3^-)$ values of 2.5±12.5‰ (Elliott et al., 2009; Freyer, 1978; Heaton, 1987) and 19±3‰ (Savarino et al., 2007), respectively. Previous modeling work of NO_3^- over Antarctica has indicated a background level of NO_3^- concentration is expected to occur during May and July, consistent with our observations (Fig.1) (Lee et al., 2014). This source of NO_3^- has been modeled to result from NO_x emissions from fossil fuel combustion, soil emissions, and lightning originating from 25º to 65 ºS that is transported to Antarctica as p-NO_3^- and HNO_3 resulting from its formation above continental source regions at an altitude of 5-11 km. (Lee et al., 2014). The slight peak in NO_3^- concentrations during August (Fig. 1) has also been modeled and has been suggested to be the result of increasing importance of long-range transported PAN and subsequent thermal decomposition and influences from stratospheric

514 denitrification (Lee et al., 2014). Both potential sources are consistent with our measured
515 $\delta^{15}N(NO_3^-)$ at the South Pole during winter. We note that while $\delta^{15}N$ values of PAN are
516 uncertain as the isotopic fractionation associated with PAN formation and decomposition are
517 unknown, these values are likely similar to the continental (or anthropogenic) NO_3^- of
518 2.5±12.5‰ (Elliott et al., 2009; Freyer, 1978; Heaton, 1987).
519
520 **4.1.2 Nitrate $\Delta^{17}O$ and $\delta^{18}O$**
521 The measured seasonal profile of $\Delta^{17}O(NO_3^-)$ matches closely with that previously
522 reported for NO_3^- aerosols collected at the South Pole in 2003 to 2004 (McCabe et al., 2007), that
523 were suggested to reflect localized tropospheric oxidation chemistry during summer and a
524 combination of stratospheric denitrification and transported nitrate from the lower latitudes
525 during winter. Tropospheric oxidation can result in a $\Delta^{17}O(NO_3^-)$ in the range of 17.3 to 42.3‰
526 that reflects NO_x cycling with O_3, RO_2 (or HO_2), and reactive halogens (XO; most notably BrO)
527 and subsequent NO_2 oxidation that may incorporate O atoms derived from O_3, H_2O, and/or OH
528 in the product NO_3^- (Michalski et al., 2003; Morin et al., 2009) (Table 1). Elevated $\Delta^{17}O(NO_3^-)$
529 values of stratospheric NO_3^- are suspected to exist due to elevated stratospheric $\Delta^{17}O(O_3)$
530 signature (Janssen, 2005) relative to tropospheric O_3 and/or elevated $ClONO_2$ $\Delta^{17}O$ signatures
531 (McCabe et al., 2007) when $ClONO_2$ is the dominant source of stratospheric nitrate during the
532 polar vortex (R1-R2):

533 $$ClO + NO_2 \longrightarrow ClONO_2 \qquad \text{(R1)}$$

534 $$ClONO_2 + HCl \longrightarrow HNO_3 + Cl_2 \qquad \text{(R2)}$$

535 This framework is consistent with the measured $\Delta^{17}O(NO_3^-)$ that was within the general
536 expected troposphere $\Delta^{17}O(NO_3^-)$ range during summer, fall, and spring (21.8 to 32.4‰),

reflecting tropospheric nitrate formation contributions by NO_2 + OH oxidation that tend to be higher during periods of sunlight due to elevated OH concentrations. The high $\Delta^{17}O(NO_3^-)$ observed during winter (41.1‰) likely reflects tropospheric nitrate formation dominated by NO_3 + RH or halogen hydrolysis during the absence of sunlight and/or stratospheric denitrification.

To further constrain NO_3^- oxidation pathways, we considered $\delta^{18}O$-$\Delta^{17}O$ spaces for major tropospheric O bearing molecules incorporated into NO_3^- (Fig. 3) (Fibiger et al., 2016; Michalski et al., 2012). Here we assume that the O isotopic composition of NO_3^- is derived from a mixture between a high $\delta^{18}O$-$\Delta^{17}O$ end-member, $O_{3(terminal)}$ and XO ($\delta^{18}O$ = 95-115‰ (Johnston & Thiemens, 1997), $\Delta^{17}O$ =39.3±2.0‰; (Vicars & Savarino, 2014) and various low $\delta^{18}O$-$\Delta^{17}O$ end-members of O bearing molecules that are incorporated into NO_3^- including $O_2/RO_2/HO_2$ ($\delta^{18}O$ = 23.5‰ $\Delta^{17}O$ = 0‰; (Kroopnick & Craig, 1972), H_2O ($\delta^{18}O$ = -27.5±20‰, $\Delta^{17}O$ = 0‰) and OH ($\delta^{18}O$ = -70±20‰, $\Delta^{17}O$ = 0). We note that OH may not attain complete isotopic equilibrium with H_2O vapor in polar regions because of low water mixing ratios (Morin et al., 2007). If OH maintains some of its O_3 character from $O(^1D)$, the mixing line between O_3 and OH remains the same, with the O atom incorporated into NO_3^- shifted towards O_3 (Fibiger et al., 2016). We note that due to the speculative nature of $\delta^{18}O$ values of some of the major O bearing molecules it can be difficult to quantitatively use this to evaluate oxidation pathways, but it may provide some additional qualitative constraints.

From $\delta^{18}O$-$\Delta^{17}O$ space, summer NO_3^- tended to be a mixture between $O_{3(term)}$ and OH, indicating that NO_3^- is primary formed through the $NO_2 + OH + M \rightarrow HNO_3 + M$ oxidation pathway. Elevated [OH] has been measured during the summer at the South Pole (as high as 2.0

560 $\times 10^6$ molecules/cm^3; (Mauldin et al., 2001)). If OH oxidation dominated summer NO_3^-
561 formation, then based on $\Delta^{17}O$ mass-balance, the starting NO_2 would have had a $\Delta^{17}O$ of 41.4‰,
562 indicating near complete NO_x cycling with O_3. This is unrealistic due to the high HO_x
563 concentration in summer in the interior of Antarctica (Savarino et al., 2016), suggesting that an
564 unknown processes appears to play a significant role on the atmospheric NO_3^- budget during
565 summer at the South Pole, which has also been reported for Dome C (Savarino et al., 2016). Fall
566 NO_3^- tended to shift towards a mixture involving $O_{3(term)}$ and O_2, which indicates incorporation of
567 O atoms derived from RO_2/HO_2 during NO_x photochemical cycling. This is consistent with
568 model results for the mid to high latitude of the Southern Hemisphere that predicts the dominant
569 post NO_2 oxidation pathways are likely a mixture between NO_2 + OH (dominant daytime) and
570 NO_3 + DMS (dominant nighttime) pathways (Alexander et al., 2009). Since the South Pole is
571 dark during this period, (i.e. absence of NO_x photochemical cycling), this suggests that some of
572 the NO_3^- during autumn is derived from long-range transport, which is consistent with the
573 $\delta^{15}N(NO_3^-)$ values measured during this collection period, conclusions drawn for NO_3^- collected
574 during the fall at DDU (Savarino et al., 2007), and model expectations (Lee et al., 2014). Winter
575 $\delta^{18}O$-$\Delta^{17}O$ space indicates that all O atoms derived from $O_{3(term)}$, suggesting that either high end-
576 member $\delta^{18}O$-$\Delta^{17}O$ tropospheric oxidation pathways (e.g. NO_3 + DMS or $XONO_2$ hydrolysis)
577 played an important role in NO_3^- formation or stratospheric denitrification. Finally, spring NO_3^-
578 tracked between $O_{3(term)}$ and RO_2 (or HO_2) and OH. We note that springtime mixing
579 relationships overlap with $O_{3(term)}$ and H_2O mixing, but the N_2O_5 hydrolysis pathway is expected
580 to play a minor role over the South Pole during this period (Alexander et al., 2009). Since
581 snowpack photolysis returns during this period of constant sunlight, local oxidation is expected
582 to dominate the NO_3^- formed at the South Pole as supported by our $\delta^{15}N(NO_3^-)$ results. This

583 indicates that RO_2 (and/or HO_2) chemistry played an important role in NO_x photochemical
584 cycling leading to elevated localized [O_3] (Crawford et al., 2001). Post NO_2 oxidation is likely a
585 mixture between daytime pathways including NO_2 + OH and $XONO_2$ hydrolysis (Alexander et
586 al., 2009). These two pathways have opposite $\delta^{18}O$-$\Delta^{17}O$ mixing end-members (e.g. Fig 4) and
587 likely explains the observed mid-ranged NO_3^- $\delta^{18}O$-$\Delta^{17}O$ values during spring.
588

589 **4.2 SO_4^{2-} Seasonal Cycle**

590 **4.2.1 $\delta^{34}S(SO_4^{2-})_{(TSP)}$**

591 Elevated $[SO_4^{2-}]_{(TSP)}$ (86.7 ± 73.7 ng/m^3, n =17) occurred during summer and fall when
592 biogenic activity was highest (January – May) and supported by an average $\delta^{34}S(SO_4^{2-})_{(TSP)}$ of
593 18.5±1.0‰ (n=10), which is indistinguishable from DMS $\delta^{34}S$ value of 18.6±1.9‰ (Patris et al.,
594 2002; Sanusi et al., 2006). Seven-day back mass-trajectories, indicate that air masses did not
595 originate over the coast of Antarctica. During winter (June-August), $[SO_4^{2-}]_{(TSP)}$ decreased to a
596 baseline level of approximately 15.3 ng/m^3 with an average $\delta^{34}S(SO_4^{2-})_{(TSP)}$ of 14.2 ± 0.9‰
597 (n=4). This decrease in $[SO_4^{2-}]_{(TSP)}$ is result of substantially less biogenic sulfur production
598 during this time-period in the Southern Hemisphere, which is supported by a decrease in
599 wintertime $\delta^{34}S(SO_4^{2-})_{(TSP)}$ indicating a relatively larger contribution from a non-biogenic
600 $\delta^{34}S(SO_4^{2-})$ source with a low end-member such as continental transport (including volcanic,
601 mineral, continental biogenic, and anthropogenic sources) (Patris et al., 2000) ($\delta^{34}S$ = 3±3‰;
602 (Jenkins & Bao, 2006; Li & Barrie, 1993; Norman et al., 1999), stratospheric intrusions ($\delta^{34}S$ =
603 2.6±0.3‰; (Castleman Jr et al., 1974), and localized passive volcanic emission of SO_2 ($\delta^{34}S$ = 0
604 to 5‰; Liotta et al., 2012). Stratospheric inputs should result in a SO_4^{2-} with an elevated
605 $\Delta^{17}O(SO_4^{2-})$ due to oxidation reactions involving OH with a modeled $\Delta^{17}O$ between 2 and 45‰

606 (Lyons, 2001), but an increase in $\Delta^{17}O(SO_4^{2-})$ was not observed during this sampling period
607 limiting this possibility. At the end of winter and early spring (September – October), $[SO_4^{2-}]_{(TSP)}$
608 increased to 29.6 ± 19.0 ng/m^3 (n = 7), and the mass-weighted $\delta^{34}S(SO_4^{2-})_{(TSP)}$ was 13.7 ±
609 1.4‰ (n = 4), which is lower that observed during winter. This again indicates the potential
610 importance of a SO_4^{2-} source with a low end-member $\delta^{34}S$ value. Previous work in the Southern
611 Ocean have indicated that spring-time $SO_4^{2-}{}_{(NSS)}$ tends to be dominated by DMS emissions (Li et
612 al., 2018). Thus, the increase in $SO_4^{2-}{}_{(TSP)}$ during this period likely reflects the increased
613 emission of DMS but relatively low $\delta^{34}S(SO_4^{2-})_{(TSP)}$ during this period highlights the importance
614 of a non-biogenic $SO_4^{2}{}_{-(TSP)}$ source with a low-end member $\delta^{34}S(SO_4^{2-})$ value. Overall, elevated
615 $\delta^{34}S(SO_4^{2-})_{(TSP)}$ throughout the year points suggests that biogenic emissions tend to dominate the
616 $SO_4^{2-}{}_{(TSP)}$ source year-round at the South Pole assuming sea-salt SO_4^{2-} contribution is negligible.
617 A relatively higher contribution from a non-biogenic SO_4^{2-} source was observed during winter
618 and spring than observed during summer and fall based on $\delta^{34}S(SO_4^{2-})_{(TSP)}$. These findings are
619 consistent with previous work in the interior of Antarctica (Concordia) that have shown that
620 biogenic-derived SO_4^{2-} tends to dominate the nss-SO_4^{2-} budget year-round based off nss-SO_4^{2-} to
621 MSA measurements (Legrand et al., 2017).
622
623 **4.2.2 $\Delta^{17}O(SO_4^{2-})$ and $\delta^{18}O(SO_4^{2-})$**
624 The measured $\Delta^{17}O(SO_4^{2-})_{(TSP)}$ values at the South Pole had a somewhat similar seasonal
625 cycle as that reported for at Dome C (Fig. 2). Typically, lowest values are observed during
626 summer ($\Delta^{17}O$ = 0.9±0.1‰; n=5) and during winter (1.0±0.2‰; n=4) reflecting greater
627 contributions from OH, H_2O_2, and HOBr (or HOCl) oxidation pathways (Fig. 5). Highest $\Delta^{17}O$
628 values occurred during autumn (1.3 ± 0.3‰, n =6) and spring (1.6±0.1‰, n=5). Since these

629 $\Delta^{17}O$ values greater than 1‰ indicate contributions from aqueous O_3 oxidation. The maximum
630 contribution from S(IV) + O_3 oxidation for each SO_4^{2-} sample was calculated assuming no
631 contribution from H_2O_2 (Eq. 3) (Chen et al., 2016):

632 $$f_{O_{3,max}} = \frac{\Delta^{17}O_{obs}(SO_4^{2-})}{\Delta^{17}O(SO_4^{2-})_{O_3}} \quad \text{(Eq. 3)}$$

633 where $\Delta^{17}O(SO_4^{2-})_{O3}$ = 9.9‰ (Table 1). In a similar manner, the minimum contribution from O_3
634 oxidation can be estimated assuming that H_2O_2 is the only other oxidation pathway (Eq. 4) (Chen
635 et al., 2016):

636 $$f_{O_{3,min}} = \frac{\Delta^{17}O_{obs}(SO_4^{2-}) - \Delta^{17}O(SO_4^{2-})_{H_2O_2}}{\Delta^{17}O(SO_4^{2-})_{O_3} - \Delta^{17}O(SO_4^{2-})_{H_2O_2}} \quad \text{(Eq. 4)}$$

637 where $\Delta^{17}O(SO_4^{2-})_{H2O2}$ = 0.7‰ (Table 1). This yields an estimated O_3 contribution range
638 (minimal to maximum) of 0.02–0.09, 0.06–0.13, 0.04–0.11, and 0.10-0.16 for summer, fall,
639 winter, and spring, respectively. This indicates that O_3 oxidation appears to have played the
640 largest role during spring and smallest role during summer (Fig. 5). A relatively minor
641 contribution from O_3 oxidaiton during summer is not surprising due to the strong role HO_x
642 chemistry and HOX plays during this period. We note that our estimate for f_{O3} for wintertime
643 $SO_4^{2-}{}_{(TSP)}$ might be influenced by a possible higher contribution from primary $SO_4^{2-}{}_{(SS)}$ during
644 this period, with a $\Delta^{17}O$ = 0‰ that we cannot accurately correct for with our dataset. Assuming
645 a similar $SO_4^{2-}{}_{(SS)}$ contribution in our samples as found at Dome C during winter of ~0.33, our
646 estimated f_{O3} range would increase to 0.09-0.16.
647
648 The observed $\delta^{18}O(SO_4^{2-})_{(TSP)}$ also exhibited somewhat of a seasonal trend, with lowest
649 values found during summer ($\delta^{18}O$ = -11.1±1.2‰) and highest values found during winter ($\delta^{18}O$
650 = 6.6±1.0‰) (Table 3). This apparent non-correlation may be driven by the isotopic
651 equilibration between SO_2 and H_2O vapor (Holt et al., 1981) (R3):

652 $$S^{16}O^{16}O + H_2{}^{18}O \rightleftharpoons S^{16}O^{18}O + H_2{}^{16}O \quad \text{(R3)}$$

653 This isotopic exchange reaction favors the partitioning of ^{18}O into SO_2 with an isotopic
654 enrichment factor that is strongly dependent on temperature, with increasing isotopic enrichment
655 factors for decreasing temperatures (Richet et al., 1977). This exchange reaction may explain the
656 moderate correlation observed between $\delta^{18}O(SO_4^{2-})_{(TSP)}$ and temperature ($R^2 = 0.59$) in which
657 $\delta^{18}O(SO_4^{2-})_{(TSP)}$ is found to increase with lower temperatures. Therefore, without having
658 knowledge of the precursor $\delta^{18}O(SO_2)$ it is currently nearly impossible to use $\delta^{18}O$-$\Delta^{17}O$ space of
659 $SO_4^{2-}{}_{(TSP)}$ to quantitatively evaluate differences in reaction pathways. However, we note that due
660 to the potential of $\delta^{18}O$-$\Delta^{17}O$ evaluation of SO_4^{2-}, future work should aim to better quantify the
661 $\delta^{18}O$-$\Delta^{17}O$ of formation pathways requiring a combination of experimental and modeling work.

662

663 **5 Conclusions**

664 Aerosol samples were collected over a ten-month period at the South Pole in 2002, and a
665 combination of concentration and isotopic analysis was used to evaluate the dynamics of NO_3^-
666 and $SO_4^{2-}{}_{(TSP)}$. NO_3^- variations were found to be driven by seasonal snowpack photolysis
667 resulting in elevated $[NO_3^-]$ levels because of localized atmospheric recycling, producing
668 relatively low $\delta^{15}N(NO_3^-)$ values (-47.0±11.7‰, n = 5) during periods of sunlight at the South
669 Pole. The seasonal cycle of $\Delta^{17}O(NO_3^-)$ at the South Pole indicates tropospheric chemistry
670 dominates NO_3^- formation year-round with possible stratospheric denitrification contributions
671 during winter. Seasonal $[SO_4^{2-}]_{(TSP)}$ had some similarities with $[NO_3^-]$, with highest values
672 during summer and lowest values during winter. Summertime elevated $[SO_4^{2-}]_{(TSP)}$ appears to be
673 derived from transported biogenic sulfur emissions as evidenced by $\delta^{34}S(SO_4^{2-})_{(TSP)}$ of
674 18.5±1.0‰ (n=10) that is near the marine biogenic $\delta^{34}S$ value. The seasonal cycle of $\Delta^{17}O(SO_4^{2-}$

675 $)_{(TSP)}$ exhibited nearly uniform values year-round (0.8 to 1.8‰) with slight seasonal variation that
676 indicated highest aqueous O_3 oxidation contributions during fall and autumn.

677

678 **Acknowledgments, Samples, and Data**

679 W.W.W. acknowledges support from an Atmospheric and Geospace Sciences National Science
680 Foundation Postdoctoral Fellow (Grant # 1624618). We acknowledge support from the Purdue
681 Center for Climate Change. The authors declare no financial conflicts of interest. We thank the
682 South Pole Observatory and the National Oceanic and Atmospheric Administration Earth System
683 Research Laboratory Global Monitoring Division for access to ancillary meteorology and ozone
684 data. Data presented in this manuscript are available within the text (Tables 2 & 3) and in the
685 Supporting Information.

686

687 **References**

688 Alexander, B., Thiemens, M. H., Farquhar, J., Kaufman, A. J., Savarino, J., & Delmas, R. J. (2003). East
689 Antarctic ice core sulfur isotope measurements over a complete glacial-interglacial cycle. *Journal*
690 *of Geophysical Research: Atmospheres*, *108*(D24).
691 Alexander, B., Savarino, J., Kreutz, K. J., & Thiemens, M. H. (2004). Impact of preindustrial biomass-
692 burning emissions on the oxidation pathways of tropospheric sulfur and nitrogen. *Journal of*
693 *Geophysical Research: Atmospheres*, *109*(D8).
694 Alexander, B., Park, R. J., Jacob, D. J., Li, Q. B., Yantosca, R. M., Savarino, J., et al. (2005). Sulfate
695 formation in sea-salt aerosols: Constraints from oxygen isotopes. *Journal of Geophysical*
696 *Research: Atmospheres*, *110*(D10).

697 Alexander, B., Hastings, M. G., Allman, D. J., Dachs, J., Thornton, J. A., & Kunasek, S. A. (2009).
698 Quantifying atmospheric nitrate formation pathways based on a global model of the oxygen
699 isotopic composition ($\Delta^{17}O$) of atmospheric nitrate. *Atmos. Chem. Phys.*, *9*(14), 5043–5056.
700 Arimoto, R., Nottingham, A. S., Webb, J., Schloesslin, C. A., & Davis, D. D. (2001). Non-sea salt sulfate
701 and other aerosol constituents at the South Pole during ISCAT. *Geophysical Research Letters*,
702 *28*(19), 3645–3648.
703 Augustin, L., Barbante, C., Barnes, P. R., Barnola, J. M., Bigler, M., Castellano, E., et al. (2004). Eight
704 glacial cycles from an Antarctic ice core. *Nature*, *429*, 623–628.
705 Barkan, E., & Luz, B. (2003). High-precision measurements of 17O/16O and 18O/16O of O2 and O2/Ar
706 ratio in air. *Rapid Communications in Mass Spectrometry*, *17*(24), 2809–2814.
707 https://doi.org/10.1002/rcm.1267
708 Barkan, E., & Luz, B. (2005). High precision measurements of $^{17}O/^{16}O$ and $^{18}O/^{16}O$ ratios in H_2O. *Rapid*
709 *Communications in Mass Spectrometry*, *19*(24), 3737–3742.
710 Barnola, J.-M., Raynaud, D., Korotkevich, Y. S., & Lorius, C. (1987). Vostok ice core provides 160,000-
711 year record of atmospheric CO_2. *Nature*, *329*(6138), 408.
712 Berhanu, T. A., Meusinger, C., Erbland, J., Jost, R., Bhattacharya, S. K., Johnson, M. S., & Savarino, J.
713 (2014). Laboratory study of nitrate photolysis in Antarctic snow. II. Isotopic effects and
714 wavelength dependence. *The Journal of Chemical Physics*, *140*(24), 244306.
715 Berhanu, T. A., Savarino, J., Erbland, J., Vicars, W. C., Preunkert, S., Martins, J. F., & Johnson, M. S.
716 (2015). Isotopic effects of nitrate photochemistry in snow: a field study at Dome C, Antarctica.
717 *Atmospheric Chemistry and Physics*, *15*(19), 11243–11256.
718 Bohlke, J. K., Gwinn, C. J., & Coplen, T. B. (1993). New reference materials for nitrogen-isotope-ratio
719 measurements. *Geostandards Newsletter*, *17*(1), 159–164.
720 Castleman Jr, A. W., Munkelwitz, H. R., & Manowitz, B. (1974). Isotopic studies of the sulfur
721 component of the stratospheric aerosol layer. *Tellus*, *26*(1–2), 222–234.

Chen, G., Davis, D., Crawford, J., Hutterli, L. M., Huey, L. G., Slusher, D., et al. (2004). A reassessment of HO_x South Pole chemistry based on observations recorded during ISCAT 2000. *Atmospheric Environment*, *38*(32), 5451–5461.

Chen, Q., Geng, L., Schmidt, J. A., Xie, Z., Kang, H., Dachs, J., et al. (2016). Isotopic constraints on the role of hypohalous acids in sulfate aerosol formation in the remote marine boundary layer. *Atmospheric Chemistry and Physics*, *16*(17), 11433–11450.

Craig, H., Chou, C. C., Welhan, J. A., Stevens, C. M., & Engelkemeir, A. (1988). The Isotopic Composition of Methane in Polar Ice Cores. *Science*, *242*(4885), 1535.

Crawford, J. H., Davis, D. D., Chen, G., Buhr, M., Oltmans, S., Weller, R., et al. (2001). Evidence for photochemical production of ozone at the South Pole surface. *Geophysical Research Letters*, *28*(19), 3641–3644.

Davis, D., Chen, G., Buhr, M., Crawford, J., Lenschow, D., Lefer, B., et al. (2004). South Pole NO_x Chemistry: an assessment of factors controlling variability and absolute levels. *Atmospheric Environment*, *38*(32), 5375–5388.

Delmas, R. J. (2013). *Ice core studies of global biogeochemical cycles* (Vol. 30). Springer Science & Business Media.

Dominguez, G., Jackson, T., Brothers, L., Barnett, B., Nguyen, B., & Thiemens, M. H. (2008). Discovery and measurement of an isotopically distinct source of sulfate in Earth's atmosphere. *Proceedings of the National Academy of Sciences*, *105*(35), 12769–12773.

Elliott, E. M., Kendall, C., Boyer, E. W., Burns, D. A., Lear, G. G., Golden, H. E., et al. (2009). Dual nitrate isotopes in dry deposition: Utility for partitioning NOx source contributions to landscape nitrogen deposition. *Journal of Geophysical Research. Biogeosciences*, *114*(4).

Erbland, J., Vicars, W. C., Savarino, J., Morin, S., Frey, M. M., Frosini, D., et al. (2013). Air–snow transfer of nitrate on the East Antarctic Plateau – Part 1: Isotopic evidence for a photolytically driven dynamic equilibrium in summer. *Atmos. Chem. Phys.*, *13*(13), 6403–6419.

747 Fibiger, D. L., Dibb Jack E., Chen Dexian, Thomas Jennie L., Burkhart John F., Huey L. Gregory, &
748 Hastings Meredith G. (2016). Analysis of nitrate in the snow and atmosphere at Summit,
749 Greenland: Chemistry and transport. *Journal of Geophysical Research: Atmospheres*, *121*(9),
750 5010–5030.
751 Fogelman, K. D., Walker, D. M., & Margerum, D. W. (1989). Nonmetal redox kinetics: hypochlorite and
752 hypochlorous acid reactions with sulfite. *Inorganic Chemistry*, *28*(6), 986–993.
753 Frey, M. M., Savarino, J., Morin, S., Erbland, J., & Martins, J. M. F. (2009). Photolysis imprint in the
754 nitrate stable isotope signal in snow and atmosphere of East Antarctica and implications for
755 reactive nitrogen cycling. *Atmospheric Chemistry and Physics*, *9*(22), 8681–8696.
756 Freyer, H. D. (1978). Seasonal trends of NH_4^+ and NO_3^- nitrogen isotope composition in rain collected at
757 Jülich, Germany. *Tellus*, *30*(1), 83–92.
758 Friedli, H., Lötscher, H., Oeschger, H., Siegenthaler, U., & Stauffer, B. (1986). Ice core record of the
759 13C/12C ratio of atmospheric CO_2 in the past two centuries. *Nature*, *324*(6094), 237–238.
760 Hastings, M. G., Jarvis, J. C., & Steig, E. J. (2009). Anthropogenic Impacts on Nitrogen Isotopes of Ice-
761 Core Nitrate. *Science*, *324*(5932), 1288–1288.
762 Hauglustaine, D. A., Balkanski, Y., & Schulz, M. (2014). A global model simulation of present and future
763 nitrate aerosols and their direct radiative forcing of climate. *Atmospheric Chemistry & Physics*,
764 *14*(5).
765 Haywood, J., & Boucher, O. (2000). Estimates of the direct and indirect radiative forcing due to
766 tropospheric aerosols: A review. *Reviews of Geophysics*, *38*(4), 513–543.
767 Heaton, T. H. E. (1987). 15N14N ratios of nitrate and ammonium in rain at Pretoria, South Africa.
768 *Atmospheric Environment (1967)*, *21*(4), 843–852.
769 Heaton, T. H. E. (1990). $^{15}N/^{14}N$ ratios of NO_x from vehicle engines and coal-fired power stations. *Tellus*
770 *B*, *42*(3), 304–307.
771 Helmig, D., Oltmans, S. J., Carlson, D., Lamarque, J.-F., Jones, A., Labuschagne, C., et al. (2007). A
772 review of surface ozone in the polar regions. *Atmospheric Environment*, *41*(24), 5138–5161.

Hill-Falkenthal, J., Priyadarshi, A., Savarino, J., & Thiemens, M. (2013). Seasonal variations in ^{35}S and $\Delta^{17}O$ of sulfate aerosols on the Antarctic plateau. *Journal of Geophysical Research: Atmospheres*, *118*(16), 9444–9455.

Holt, B. D., Kumar, R., & Cunningham, P. T. (1981). Oxygen-18 study of the aqueous-phase oxidation of sulfur dioxide. *Atmospheric Environment (1967)*, *15*(4), 557–566.

Ishino, S., Hattori, S., Savarino, J., Jourdain, B., Preunkert, S., Legrand, M., et al. (2017). Seasonal variations of triple oxygen isotopic compositions of atmospheric sulfate, nitrate, and ozone at Dumont d'Urville, coastal Antarctica. *Atmos. Chem. Phys.*, *17*(5), 3713–3727.

Janssen, C. (2005). Intramolecular isotope distribution in heavy ozone ($^{16}O^{18}O^{16}O$ and $^{16}O^{16}O^{18}O$). *Journal of Geophysical Research: Atmospheres (1984–2012)*, *110*(D8).

Jenkins, K. A., & Bao, H. (2006). Multiple oxygen and sulfur isotope compositions of atmospheric sulfate in Baton Rouge, LA, USA. *Atmospheric Environment*, *40*(24), 4528–4537.

Johnston, J. C., & Thiemens, M. H. (1997). The isotopic composition of tropospheric ozone in three environments. *Journal of Geophysical Research: Atmospheres (1984–2012)*, *102*(D21), 25395–25404.

Kaiser, J., Röckmann, T., & Brenninkmeijer, C. A. (2004). Contribution of mass-dependent fractionation to the oxygen isotope anomaly of atmospheric nitrous oxide. *Journal of Geophysical Research: Atmospheres*, *109*(D3).

Kiehl, J. T., Schneider, T. L., Rasch, P. J., Barth, M. C., & Wong, J. (2000). Radiative forcing due to sulfate aerosols from simulations with the National Center for Atmospheric Research Community Climate Model, Version 3. *Journal of Geophysical Research: Atmospheres*, *105*(D1), 1441–1457.

Krankowsky, D., Bartecki, F., Klees, G. G., Mauersberger, K., Schellenbach, K., & Stehr, J. (1995). Measurement of heavy isotope enrichment in tropospheric ozone. *Geophysical Research Letters*, *22*(13), 1713–1716.

Kroopnick, P., & Craig, H. (1972). Atmospheric oxygen: isotopic composition and solubility fractionation. *Science*, *175*(4017), 54–55.

Lee, C. C.-W., & Thiemens, M. H. (2001). The $\delta^{17}O$ and $\delta^{18}O$ measurements of atmospheric sulfate from a coastal and high alpine region: A mass-independent isotopic anomaly. *Journal of Geophysical Research: Atmospheres*, *106*(D15), 17359–17373.

Lee, H.-M., Henze, D. K., Alexander, B., & Murray, L. T. (2014). Investigating the sensitivity of surface-level nitrate seasonality in Antarctica to primary sources using a global model. *Atmospheric Environment*, *89*, 757–767.

Legrand, M., Preunkert, S., Weller, R., Zipf, L., Elsässer, C., Merchel, S., et al. (2017). Year-round record of bulk and size-segregated aerosol composition in central Antarctica (Concordia site) Part 2: Biogenic sulfur (sulfate and methanesulfonate) aerosol. *Atmospheric Chemistry and Physics*, *17*, 14055–14073.

Legrand, M. R., Lorius, C., Barkov, N. I., & Petrov, V. N. (1988). Vostok (Antarctica) ice core: atmospheric chemistry changes over the last climatic cycle (160,000 years). *Atmospheric Environment (1967)*, *22*(2), 317–331.

Legrand M., Preunkert S., Jourdain B., Gallée H., Goutail F., Weller R., & Savarino J. (2009). Year- round record of surface ozone at coastal (Dumont d'Urville) and inland (Concordia) sites in East Antarctica. *Journal of Geophysical Research: Atmospheres*, *114*(D20).

Leuenberger, M., Siegenthaler, U., & Langway, C. (1992). Carbon isotope composition of atmospheric CO2 during the last ice age from an Antarctic ice core. *Nature*, *357*(6378), 488.

Li, J., Michalski, G., Davy, P., Harvey, M., Katzman, T., & Wilkins, B. (2018). Investigating Source Contributions of Size-Aggregated Aerosols Collected in Southern Ocean and Baring Head, New Zealand Using Sulfur Isotopes. *Geophysical Research Letters*, *45*(8), 3717–3727.

Li, S.-M., & Barrie, L. A. (1993). Biogenic sulfur aerosol in the Arctic troposphere: 1. Contributions to total sulfate. *Journal of Geophysical Research: Atmospheres*, *98*(D11), 20613–20622.

Liu, Q., Schurter, L. M., Muller, C. E., Aloisio, S., Francisco, J. S., & Margerum, D. W. (2001). Kinetics and Mechanisms of Aqueous Ozone Reactions with Bromide, Sulfite, Hydrogen Sulfite, Iodide, and Nitrite Ions. *Inorganic Chemistry*, *40*(17), 4436–4442.

825 Lyons, J. R. (2001). Transfer of mass-independent fractionation in ozone to other oxygen-containing
826 radicals in the atmosphere. *Geophysical Research Letters*, *28*(17), 3231–3234.
827 MacFarling Meure, C., Etheridge, D., Trudinger, C., Steele, P., Langenfelds, R., Van Ommen, T., et al.
828 (2006). Law Dome CO2, CH4 and N2O ice core records extended to 2000 years BP. *Geophysical*
829 *Research Letters*, *33*(14).
830 Mauldin, R. L., Eisele, F. L., Tanner, D. J., Kosciuch, E., Shetter, R., Lefer, B., et al. (2001).
831 Measurements of OH, H_2SO_4, and MSA at the South Pole during ISCAT. *Geophysical Research*
832 *Letters*, *28*(19), 3629–3632.
833 McCabe, J. R., Thiemens, M. H., & Savarino, J. (2007). A record of ozone variability in South Pole
834 Antarctic snow: Role of nitrate oxygen isotopes. *Journal of Geophysical Research: Atmospheres*,
835 *112*(D12), D12303.
836 Michalski, G., Savarino, J., Böhlke, J. K., & Thiemens, M. (2002). Determination of the Total Oxygen
837 Isotopic Composition of Nitrate and the Calibration of a $\Delta^{17}O$ Nitrate Reference Material.
838 *Analytical Chemistry*, *74*(19), 4989–4993.
839 Michalski, G., Scott, Z., Kabiling, M., & Thiemens, M. H. (2003). First measurements and modeling of
840 $\Delta^{17}O$ in atmospheric nitrate. *Geophysical Research Letters*, *30*(16), 1870.
841 Michalski, G., Bockheim, J. G., Kendall, C., & Thiemens, M. (2005). Isotopic composition of Antarctic
842 Dry Valley nitrate: Implications for NOy sources and cycling in Antarctica. *Geophysical*
843 *Research Letters*, *32*(13).
844 Michalski, G., Bhattacharya, S. K., & Mase, D. F. (2012). Oxygen isotope dynamics of atmospheric
845 nitrate and its precursor molecules. In *Handbook of environmental isotope geochemistry* (pp.
846 613–635). Springer.
847 Morin, S., Savarino, J., Bekki, S., Gong, S., & Bottenheim, J. W. (2007). Signature of Arctic surface
848 ozone depletion events in the isotope anomaly ($\Delta^{17}O$) of atmospheric nitrate. *Atmospheric*
849 *Chemistry and Physics*, *7*(5), 1451–1469.

Morin, S., Savarino, J., Frey, M. M., Yan, N., Bekki, S., Bottenheim, J. W., & Martins, J. M. (2008). Tracing the origin and fate of NOx in the Arctic atmosphere using stable isotopes in nitrate. *Science*, *322*(5902), 730–732.

Morin, S., Savarino, J., Frey, M. M., Domine, F., Jacobi, H.-W., Kaleschke, L., & Martins, J. M. F. (2009). Comprehensive isotopic composition of atmospheric nitrate in the Atlantic Ocean boundary layer from 65°S to 79°N. *Journal of Geophysical Research: Atmospheres*, *114*(D5), D05303.

Morin, S., Sander, R., & Savarino, J. (2011). Simulation of the diurnal variations of the oxygen isotope anomaly (Δ 17 O) of reactive atmospheric species. *Atmospheric Chemistry and Physics*, *11*(8), 3653–3671.

Nielsen, H. (1974). Isotopic composition of the major contributors to atmospheric sulfur. *Tellus*, *26*(1–2), 213–221.

Norman, A. L., Barrie, L. A., Toom-Sauntry, D., Sirois, A., Krouse, H. R., Li, S. M., & Sharma, S. (1999). Sources of aerosol sulphate at Alert: Apportionment using stable isotopes. *Journal of Geophysical Research: Atmospheres*, *104*(D9), 11619–11631.

Patris, N., Delmas, R. J., & Jouzel, J. (2000). Isotopic signatures of sulfur in shallow Antarctic ice cores. *Journal of Geophysical Research: Atmospheres*, *105*(D6), 7071–7078.

Patris, N., Delmas, R., Legrand, M., De Angelis, M., Ferron, F. A., Stiévenard, M., & Jouzel, J. (2002). First sulfur isotope measurements in central Greenland ice cores along the preindustrial and industrial periods. *Journal of Geophysical Research: Atmospheres*, *107*(D11).

Preunkert, S., Jourdain, B., Legrand, M., Udisti, R., Becagli, S., & Cerri, O. (2008). Seasonality of sulfur species (dimethyl sulfide, sulfate, and methanesulfonate) in Antarctica: Inland versus coastal regions. *Journal of Geophysical Research: Atmospheres*, *113*(D15).

Rees, C. E., Jenkins, W. J., & Monster, J. (1978). The sulphur isotopic composition of ocean water sulphate. *Geochimica et Cosmochimica Acta*, *42*(4), 377–381.

875 Richet, P., Bottinga, Y., & Janoy, M. (1977). A review of hydrogen, carbon, nitrogen, oxygen, sulphur,
876 and chlorine stable isotope enrichment among gaseous molecules. *Annual Review of Earth and*
877 *Planetary Sciences*, *5*, 65–110.
878 Röthlisberger, R., Hutterli, M. A., Sommer, S., Wolff, E. W., & Mulvaney, R. (2000). Factors controlling
879 nitrate in ice cores: Evidence from the Dome C deep ice core. *Journal of Geophysical Research:*
880 *Atmospheres*, *105*(D16), 20565–20572.
881 Sanusi, A. A., Norman, A.-L., Burridge, C., Wadleigh, M., & Tang, W.-W. (2006). Determination of the
882 S isotope composition of methanesulfonic acid. *Analytical Chemistry*, *78*(14), 4964–4968.
883 Savarino, J., & Thiemens, M. H. (1999). Analytical procedure to determine both $\delta^{18}O$ and $\delta^{17}O$ of H_2O_2 in
884 natural water and first measurements. *Atmospheric Environment*, *33*(22), 3683–3690.
885 Savarino, J., Lee, C. C., & Thiemens, M. H. (2000). Laboratory oxygen isotopic study of sulfur (IV)
886 oxidation: Origin of the mass-independent oxygen isotopic anomaly in atmospheric sulfates and
887 sulfate mineral deposits on Earth. *Journal of Geophysical Research: Atmospheres*, *105*(D23),
888 29079–29088.
889 Savarino, J., Alexander, B., Darmohusodo, V., & Thiemens, M. H. (2001). Sulfur and oxygen isotope
890 analysis of sulfate at micromole levels using a pyrolysis technique in a continuous flow system.
891 *Analytical Chemistry*, *73*(18), 4457–4462.
892 Savarino, J., Bekki, S., Cole-Dai, J., & Thiemens, M. H. (2003). Evidence from sulfate mass independent
893 oxygen isotopic compositions of dramatic changes in atmospheric oxidation following massive
894 volcanic eruptions. *Journal of Geophysical Research: Atmospheres*, *108*(D21).
895 Savarino, J., Kaiser, J., Morin, S., Sigman, D. M., & Thiemens, M. H. (2007). Nitrogen and oxygen
896 isotopic constraints on the origin of atmospheric nitrate in coastal Antarctica. *Atmospheric*
897 *Chemistry and Physics*, *7*(8), 1925–1945.
898 Savarino, J., Morin, S., Erbland, J., Grannec, F., Patey, M. D., Vicars, W., et al. (2013). Isotopic
899 composition of atmospheric nitrate in a tropical marine boundary layer. *Proceedings of the*
900 *National Academy of Sciences*, *110*(44), 17668–17673.

Savarino, J., Vicars, W. C., Legrand, M., Preunkert, S., Jourdain, B., Frey, M. M., et al. (2016). Oxygen isotope mass balance of atmospheric nitrate at Dome C, East Antarctica, during the OPALE campaign. *Atmos. Chem. Phys.*, *16*(4), 2659–2673.

Shaheen, R., Abauanza, M., Jackson, T. L., McCabe, J., Savarino, J., & Thiemens, M. H. (2013). Tales of volcanoes and El-Niño southern oscillations with the oxygen isotope anomaly of sulfate aerosol. *Proceedings of the National Academy of Sciences*, *110*(44), 17662–17667.

Shaw, G., E. (2010). Antarctic aerosols: A review. *Reviews of Geophysics*, *26*(1), 89–112.

Stein, A. F., Draxler, R. R., Rolph, G. D., Stunder, B. J., Cohen, M. D., & Ngan, F. (2015). NOAA's HYSPLIT atmospheric transport and dispersion modeling system. *Bulletin of the American Meteorological Society*, *96*(12), 2059–2077.

Stohl, A., & Sodemann, H. (2010). Characteristics of atmospheric transport into the Antarctic troposphere. *Journal of Geophysical Research: Atmospheres*, *115*(D2).

Troy, R. C., & Margerum, D. W. (1991). Non-metal redox kinetics: Hypobromite and hypobromous acid reactions with iodide and with sulfite and the hydrolysis of bromosulfate. *Inorganic Chemistry*, *30*(18), 3538–3543.

Varotsos, C. (2002). The southern hemisphere ozone hole split in 2002. *Environmental Science and Pollution Research*, *9*(6), 375–376.

Vicars, W. C., & Savarino, J. (2014). Quantitative constraints on the 17 O-excess ($\Delta^{17}O$) signature of surface ozone: Ambient measurements from 50° N to 50° S using the nitrite-coated filter technique. *Geochimica et Cosmochimica Acta*, *135*, 270–287.

Vicars, W. C., Bhattacharya, S. K., Erbland, J., & Savarino, J. (2012). Measurement of the 17O-excess (Δ17O) of tropospheric ozone using a nitrite-coated filter. *Rapid Communications in Mass Spectrometry*, *26*(10), 1219–1231.

Wagenbach, D. (1996). Coastal Antarctica: Atmospheric Chemical Composition and Atmospheric Transport. In *Chemical Exchange Between the Atmosphere and Polar Snow* (pp. 173–199). Springer, Berlin, Heidelberg.

927 Weller, R., Legrand, M., & Preunkert, S. (2018). Size distribution and ionic composition of marine
928 summer aerosol at the continental Antarctic site Kohnen. *Atmospheric Chemistry and Physics*,
929 *18*(4), 2413–2430.
930 Wendler, G., & Kodama, Y. (1984). On the climate of Dome C, Antarctica, in relation to its geographical
931 setting. *International Journal of Climatology*, *4*(5), 495–508.
932 Weston Jr, R. E. (2006). When is an isotope effect non-mass dependent? *Journal of Nuclear Science and*
933 *Technology*, *43*(4), 295–299.
934 Young, E. D., Galy, A., & Nagahara, H. (2002). Kinetic and equilibrium mass-dependent isotope
935 fractionation laws in nature and their geochemical and cosmochemical significance. *Geochimica*
936 *et Cosmochimica Acta*, *66*(6), 1095–1104.
937